Research Article

A Study of the Far Infrared Spectrum of N-Acetyl-D-Glucosamine Using THz-TDS, FTIR, and Semiempirical Quantum Chemistry Methods

Pedro Chamorro-Posada,[1] Iosody Silva-Castro,[2] José Vázquez-Cabo,[3] Pablo Martín-Ramos,[4] José María López-Santos,[3] and Jesús Martín-Gil[2]

[1]*Departamento de Teoría de la Señal y Comunicaciones e IT, Universidad de Valladolid, ETSI Telecomunicación, Paseo Belén 15, 47011 Valladolid, Spain*

[2]*Laboratorio de Materiales Avanzados, ETSIIAA, Universidad de Valladolid, Avenida de Madrid 44, 34004 Palencia, Spain*

[3]*Departamento de Teoría de la Señal y Comunicaciones, Universidad de Vigo, ETSI Telecomunicación, Lagoas Marcosende s/n, 36310 Vigo, Spain*

[4]*EPSH, Universidad de Zaragoza, Carretera de Cuarte s/n, 22071 Huesca, Spain*

Correspondence should be addressed to Pedro Chamorro-Posada; pedcha@tel.uva.es
and Jesús Martín-Gil; jesusmartingil@gmail.com

The far infrared spectrum of N-acetyl-D-glucosamine has been studied by combining THz–TDS and FTIR characterization techniques with theoretical studies based on semiempirical quantum chemistry methods. A strong spectral peak at $60\,\text{cm}^{-1}$ has been identified, which constitutes the main signature of the material in the terahertz band. Calculated molecular vibrations are in good qualitative and semiquantitative agreement with both the THz-TDS and FTIR experiments. In comparison to previous DFT-based studies, the semiempirical approach chosen herein, suitable for parallel multi-core and GPU acceleration, allows for a full study using periodic boundary conditions and no further approximations within a constrained computing time.

1. Introduction

N-Acetyl-D-glucosamine (or D-GlcNAc or NAG) is a derivatized glucose monomer found in polymers of bacterial cell walls, chitin, hyaluronic acids, and various glycans. As the monomeric unit of chitin polymer, it forms the outer coverings of insects and marine crustaceans and it is the major component of the cell walls of most fungi. Chitosan (deacetyl chitin) is a form of N-acetyl glucosamine that has been chemically altered.

N-Acetyl-D-glucosamine derivatives, chitin and chitosan, have become of great interest not only as underutilized resources, but also as new functional materials of high potential in various fields [1–3]: in biomedical applications (antimicrobial agents, drug and gene delivery, wound dressings, and tissue engineering), in waste water treatment (purification and toxic ion removal), in agriculture (seed coatings and controlled agrochemical release), in food industry (packaging and preservative materials), and in cosmetics, to name a few.

The structure of N-acetyl-D-glucosamine [4] is shown in Figure 1. Crystals are monoclinic, with space group P2$_1$ and unit cell parameters $a = 11.25\,\text{Å}$, $b = 4.82\,\text{Å}$, $c = 9.72\,\text{Å}$, and $\beta = 113.7°$. Mercury software package [5] has been used for the representation.

The far infrared (FIR) spectra of polycrystalline mono- and polysaccharides are dominated by lattice modes involving molecular hydrogen bonds or/and van der Waals forces. Therefore, FIR spectroscopy techniques in general and, particularly, terahertz time domain spectroscopy (THz-TDS) are notably useful in the structural characterization of carbohydrates [6–8].
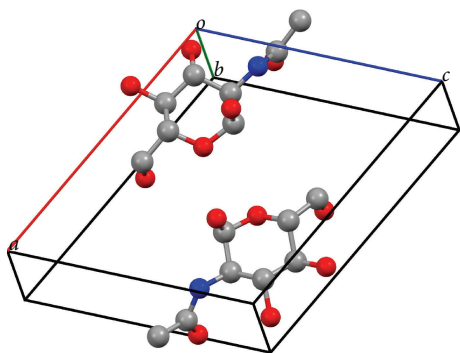
Figure 1: Crystal cell of *N*-acetyl-D-glucosamine.

Computational quantum chemistry is a highly valuable tool for the interpretation of FIR spectra due to the complexity of the associated vibration modes. *Ab initio* and density functional theory (DFT) methods are very accurate in the prediction of molecular vibrations [9]. Nevertheless, solid-state calculations over large supramolecular systems are typically required due to the relevance of long-range interactions, thus limiting the use of these computationally costly methods. On the other hand, semiempirical methods [10, 11], especially with the recently developed parallel implementations for shared-memory multiprocessor and massively parallel graphics processing units architectures [12], permit studying of the vibrations in large molecular crystals at reduced computation times. Semiempirical quantum chemistry methods have been previously used in the interpretation of the terahertz spectra of various carbon nitride [13] and carbon [14] materials.

A study of the IR spectrum of NAG was previously presented in [15]. The experimental characterization was performed using a FTIR spectrometer and the theoretical modeling using a DFT method. Due to the high computer cost of such calculations, a single molecule was studied and the intermolecular hydrogen bond interactions were simulated with intramolecular interactions. In this work, we focus on the far infrared spectrum of NAG. We combine THz–TDS and FTIR techniques for the characterization of the spectral regions between $10\,cm^{-1}$ and $80\,cm^{-1}$ and $80\,cm^{-1}$ and $420\,cm^{-1}$, respectively. THz-TDS measurements have permitted identifying one strong spectral peak at $60\,cm^{-1}$, which is the main signature of the material in the terahertz band. Theoretical studies have been performed using semiempirical quantum chemistry methods. The use of parallel multicore and GPU acceleration allows for a full study using periodic boundary conditions and no further approximations within a constrained computing time.

2. Materials and Experimental and Theoretical Methods

2.1. Materials. N-Acetyl-D-glucosamine (CAS number 7512-17-6, ≥99%) was purchased from Sigma-Aldrich Chemie GmbH (Schnelldorf, Germany). The sample material was mixed with ultrahigh molecular weight surface-modified, 53–75 μm particle size polyethylene (PE, CAS number 9002-88-4), also from Sigma-Aldrich, at 18 wt%. The mixture was pressed at 5 tm for 3 minutes to make a 13 mm diameter pellet.

2.2. Spectroscopic Characterization. A Menlo (Martinsried, Germany) Tera K15 spectrometer was used for the THz-TDS analysis. The system is based on a 1560 nm fiber laser that generates 90 fs pulses at a repetition rate of 100 MHz. This provides a compact fiber-coupled setup. The system was operated in a nitrogen-rich atmosphere in order to avoid the signature of water absorption in the recorded samples. Ten samples and ten reference measurements were performed in each case in order to reduce the noise in the measurements.

The material parameters in the spectral range of interest were calculated from the time domain photocurrent traces measured with the spectrometer. These time domain waveforms depend not only on the material data but also on the width of the pellets, due to the contributions from multiple reflections at the pellet-air interfaces. Signal processing techniques similar to those described by Duvillaret et al. [16], with a flat-top window [17], were employed in order to obtain the THz spectra of the materials.

The vibrational spectrum of the material in the 80–$420\,cm^{-1}$ spectral range was measured using a Thermo Scientific (Waltham, MA, USA) Nicolet iS50 FTIR Spectrometer. At shorter wavelengths the measurement was saturated because of the attenuation associated to the PE matrix.

2.3. Quantum Chemistry Computations. The semiempirical quantum chemistry computations were performed with the PM6 method [18] using the parallel implementation for multithreaded shared-memory CPUs and massively parallel GPU acceleration [12] of the MOPAC2012 [19] software package. A Fedora Linux server with a 12-core Intel Xeon processor and a NVIDIA Tesla K20 GPU were used for the computations.

3. Results and Discussion

3.1. FIR Spectrum of N-Acetyl-D-Glucosamine. The results of the THz-TDS measurements are shown in Figure 2. The solid line corresponds to the spectrum of the NAG sample dispersed in PE powder in the spectral range from 20 to $80\,cm^{-1}$, characterized by a dominant peak at $60\,cm^{-1}$. Two very weak peaks can also be observed at $45\,cm^{-1}$ and $72\,cm^{-1}$. The dashed line corresponds to a reference PE sample that displays a negligible attenuation in this band, even though an extremely faint absorption band near $80\,cm^{-1}$ [20] can still be observed.

The FTIR measurement results in the spectral range from $80\,cm^{-1}$ to $420\,cm^{-1}$ are shown in Figure 3. The solid line corresponds to the sample material dispersed in PE powder and the dashed line to a pure polyethylene reference pellet of similar thickness. The polyethylene attenuation displays the expected scattering response, associated with the finite particle size, and the PE band at $110\,cm^{-1}$ [20]. A second faint PE absorption band was also found close to
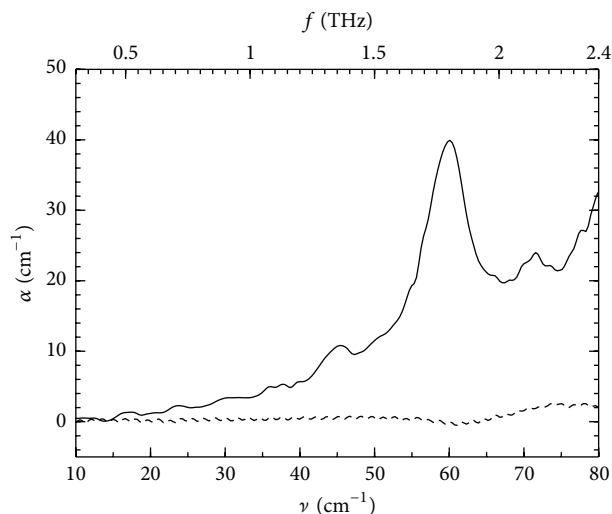
FIGURE 2: THz-TDS measurement results. The solid line corresponds to *N*-acetyl-D-glucosamine dispersed in polyethylene powder at 18 wt% and the dashed line to a reference pellet of pure polyethylene.

FIGURE 4: Measured FTIR absorbance (*dashed blue line*) and effective absorbance data after removal of the etalon effects from THz-TDS measurement (*red solid line*).

FIGURE 3: FTIR spectrum in the spectral range from $80\,\mathrm{cm^{-1}}$ to $420\,\mathrm{cm^{-1}}$. The solid line corresponds to *N*-acetyl-D-glucosamine dispersed in polyethylene powder at 18 wt% and the dashed line to a reference pellet of pure polyethylene of similar thickness.
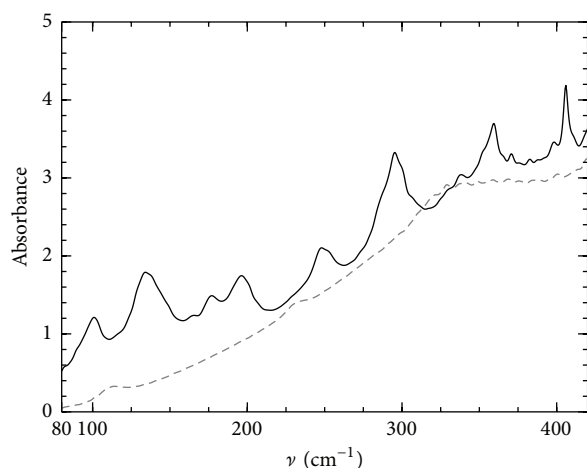
$230\,\mathrm{cm^{-1}}$. Whereas the PE matrix shows a negligible effect in the measurements below $80\,\mathrm{cm^{-1}}$, this is not the case at higher frequencies. Even though the absorption bands of the PE do not interfere at all with the spectral fingerprint of NAG, with much more defined and stronger resonances, the scattering due to the finite size of PE grains has the effect of upshifting the baseline of the measured spectrum. Moreover, the combined effect of scattering due to the finite-sized PE grains and the highly dispersive refractive index of NAG close to the resonances, known as Christiansen effect [21], can distort the shapes of the resonances and produce small shifts in the measured peaks.

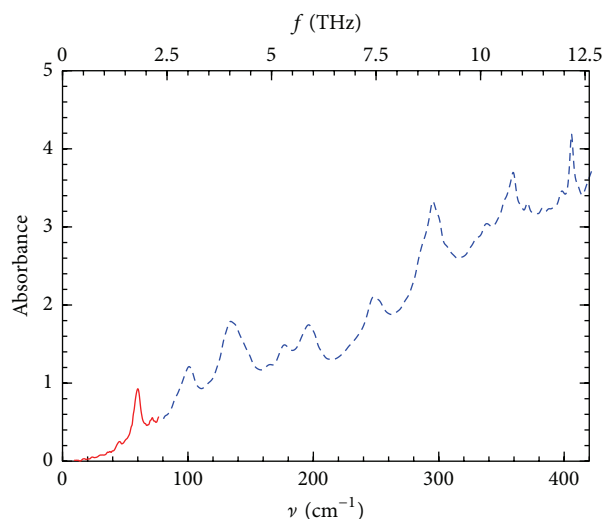The spectrum of the sample in the whole range is shown in Figure 4, where the attenuation coefficient measured with the THz-TDS spectrometer after removal of the etalon effects (as shown in Figure 2) has been converted to an effective absorbance as

$$A = \log_{10}\left[\exp\left(\alpha L\right)\right], \qquad (1)$$

where α is the attenuation coefficient in $\mathrm{cm^{-1}}$ and L is the thickness of the pellet in cm.

3.2. Semiempirical Quantum Chemistry Results. The solid-state geometry of NAG was optimized using the PM6 Hamiltonian [18] taking the actual crystal geometry [4] as the initial condition. Accurate calculations using MOPAC with periodic boundary conditions require a computational domain at least capable of fitting a sphere with a diameter of 8 Å. A minimal domain spanning $1 \times 2 \times 1$ crystal unit cells was used by setting the keyword MERS = (1, 2, 1). The unit cell dimensions of the resulting optimized geometry $a = 11.400$ Å, $b = 4.616$ Å, and $c = 9.040$ Å were in relatively good agreement with the actual values $a = 11.25$ Å, $b = 4.82$ Å, and $c = 9.72$ Å. Nevertheless, the cell angles $\alpha = 94.56°$, $\beta = 114.09°$, and $\gamma = 85.51°$ showed a noticeable deviation from the monoclinic unit cell, even though β was very close to the experimental value of 113.7°. The calculated vibrations for the crystal geometry optimized with the PM6 Hamiltonian did not include any imaginary frequency. PM7 [22] calculations provided a better fit with the actual crystal unit cell angles, but the method failed to converge to a true ground state geometry.

The PM6 geometry of one of the two molecules of the crystal unit cell is compared with the experimental structure in Figure 5. The two molecules have been plotted using VMD [23]. A relative shift has been introduced to facilitate the visual comparison due to the highly overlapping geometries. Bond lengths are compared in Table 1, and angles are compared in Table 2. We have used the atom labels shown in Figure 6.
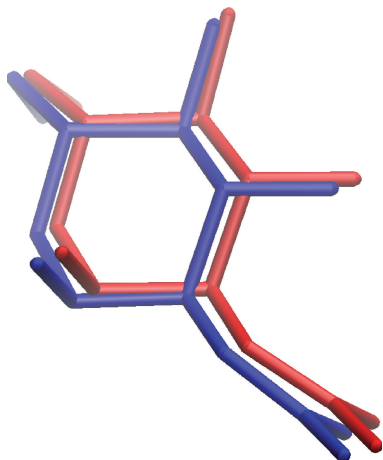
FIGURE 5: Comparison of the PM6 optimized geometry with the experimental X-ray geometry of *N*-acetyl-D-glucosamine.

TABLE 1: Comparison of the experimental bond lengths (in Å) with those of the geometry optimized with the PM6 method. The unsigned mean error (UME) is 1.30%.

Bond	Experimental distance	PM6-calculated distance	Error
C1-C2	1.5281	1.5499	1.43%
C2-C3	1.5367	1.5477	0.72%
C3-C4	1.5344	1.5464	0.78%
C4-C5	1.5504	1.5392	0.72%
C5-C6	1.5201	1.5298	0.64%
C7-C8	1.5126	1.4903	1.47%
C2-N1	1.4763	1.4745	0.12%
C7-N1	1.3800	1.3819	0.14%
C1-O1	1.3935	1.4167	1.66%
C3-O2	1.4511	1.4319	1.32%
C4-O3	1.4685	1.4382	2.06%
C1-O4	1.4593	1.4248	2.36%
C5-O4	1.4598	1.4581	0.12%
C6-O5	1.3908	1.4402	3.55%
C7-O6	1.2177	1.2465	2.37%

TABLE 2: Comparison of the experimental bond angles (in degrees) with those of the geometry optimized with the PM6 method. UME = 1.54%.

Angle	Experimental	PM6	Error
C2-C1-O1	108.33	107.52	0.75%
C2-C1-O4	108.01	111.06	2.82%
O1-C1-O4	107.95	108.7	0.69%
C1-C2-C3	110.61	109.53	0.98%
C1-C2-N1	108.92	109.16	0.22%
C3-C2-N1	108.17	111.48	3.06%
C2-C3-C4	108.60	110.39	1.65%
C2-C3-O2	108.19	108.51	0.30%
C4-C3-O2	105.90	105.73	0.16%
C3-C4-C5	106.85	110.18	3.12%
C3-C4-O3	107.75	109.13	1.28%
C5-C4-O3	105.94	106.38	0.42%
C4-C5-C6	113.88	115.29	1.24%
C4-C5-O4	105.53	108.03	2.37%
C6-C5-O4	104.94	104.08	0.82%
C5-C6-O5	111.44	110.08	1.22%
C8-C7-N1	113.15	118.45	4.68%
C8-C7-O6	123.10	120.88	1.80%
N1-C7-O6	123.62	120.59	2.45%
C2-N1-C7	119.01	121.15	1.80%
C1-O4-C5	116.51	117.14	0.54%
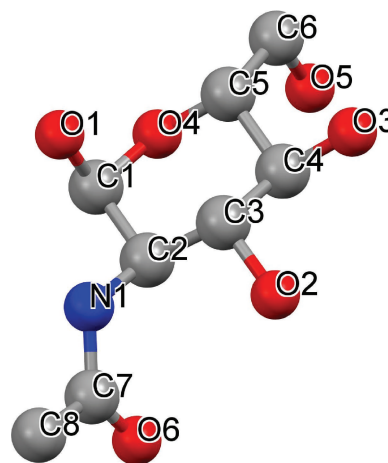
FIGURE 6: Atom labels used in the comparison of the molecular geometries.

The use of two crystal cells for the calculation of the vibrations resulted in the inclusion of modes with wave vectors sampling different points of the first Brillouin zone of the crystal. Nevertheless, only $k \cong 0$ solutions are relevant for the optical spectrum [24]. The in-phase oscillating modes were selected from the global set of vibrations [24] by projecting the mass-scaled eigenvectors components of the two cells in the computation domain and selecting only those vibrations for which the scalar product was larger than 0.9.

3.3. Frequency Assignment. The frequency assignment from our experimental and theoretical analysis is shown in Table 3, where the results are compared with those of the former study by Kovács et al. [15]. Due to the complexity of many of the vibration modes, a graphical description has been included

in Figure 7, where the mass-scaled eigenvectors are plotted for one of the molecules in the crystal cell.

In our assignment, the calculated results are in good qualitative and semiquantitative agreement with the experiments. We find larger errors for modes with a strong lattice-type vibration contribution, where the whole molecules experience large displacement. This is the case, for example, in the lowest band of the spectrum. This is typical of calculations using semiempirical and other quantum chemistry methods [24]. On the other hand, very good agreement is

Table 3: Frequency assignment and comparison with the theoretical and experimental results of [15]. The following abbreviations have been used in the description of the vibrations: s, strong; m, medium; w, weak; sh, shoulder; ν, stretching; β, in-plane bending; δ, deformation; ω, wagging; τ, twisting.

| Experimental [this work] | | | | PM6 | Experimental [15] | | DFT [15] | Characterization [15] |
FTIR		THz-TDS			FTIR			
406	m			410	404	m	397	42% δ_{ring}, 21% τCO, 10% νCO
398	w			394				
388 383	w			386				
359	m			360	359	m	373	30% wCO, 13% wCC$_{CH2}$, 13% νCC, 10% βCO$_{CH2}$
338 324	w			315	336	w	320	20% βCN, 14% νCC, 12% δ_{ring}, 12% wCO, 11% βCO$_{CH2}$, 11% βCO
296	s			301	295	s	300	33% βCO, 21% νCC, 15% βCN
274	sh			269	274	sh	277	30% wCN, 22% βCO, 10% νCC, 10% βCN
252	sh			258				
248	m			235	251	m	251	48% βCO, 26% βCN
				230	242	sh	236	26% βCN, 23% βCO, 24% δ_{ring}
196	m			225	195	m	218	41% τ_{ring}, 10% βCN, 10% τCN, 10% wCO
177	m			216	175	m	181	28% βCC$_{CH2}$, 17% βCN, 13% δ_{ring}, 10% βCO$_{CH2}$
166	w			165				
134	s			144	135	s	140	30% τ_{ring}, 18% wNH, 10% wCO, 10% τCN
101	m			100	100	m	120	42% τCH$_2$, 21% βCN, 18% τ_{ring}
90	sh			95				
82	sh			86	84	sh	86	24% τCH$_3$, 24% τ_{ring}, 21% τCN, 13% τCH$_2$
70	w	72	w	80 (76)	70	w	65	33% τCN, 23% wNH, 18% τ_{ring}
59	m	60	m	70 (63)	58	w	51	43% τ_{ring}, 42% βCN
		45	w	(45)				

found when the strongest contributions are due to localized intramolecular vibrations. This is the case, for instance, in the upper band between 350 cm^{-1} and 420 cm^{-1}. These results can be attributed to the highly accurate molecular geometry predicted with the PM6 Hamiltonian and, on the other hand, to the slightly distorted predicted crystal unit cell. The small distortion of the spectral response due to the Christiansen effect [21] could also contribute to the small discrepancies observed with the experimental measurements.

There is also good agreement between the description of [15] and our results. One difference is the signature peak at 60 cm^{-1}, which we have relabeled as being of medium (instead of weak) intensity. In our measurements, we have not observed the shoulder at 242 cm^{-1} detected in [15] and the resonance at 251 cm^{-1} in [15] is resolved in our measurements into two components: one peak at 248 cm^{-1} and a shoulder at 252 cm^{-1}. The weak PE band at 230 cm^{-1} does not seem to affect these assignments. Moreover, there are two new weak peaks between 360 cm^{-1} and 410 cm^{-1} that had not been previously measured and assigned. The lowest lying weak resonance at 45 cm^{-1} had not been previously reported and we have not been able to assign it to any of the calculated modes.

In order to improve the theoretical description in the terahertz band, we performed a geometry optimization with the PM6 method keeping the crystal cell parameters constant.

In general, optimization with this type of constraint does not guarantee that the resulting geometry is a true ground state. Nevertheless, no imaginary frequencies were found for this geometry. Besides keeping the actual crystal parameters, the quality of the molecular geometry was comparable in terms of their respective UME for bonds and angles to that of the former optimization. The results, which are shown in brackets in Table 3, permitted assigning the resonance at 45 cm^{-1} after some relaxation of the selection criterion for in-phase resonances and improving the accuracy in the assignment in the terahertz band, but a worsening was observed in the description for frequencies above 80 cm^{-1}.

4. Conclusions

A combination of THz–TDS and FTIR spectroscopies with theoretical studies based on semiempirical quantum chemistry methods has been used to study the far infrared spectrum of N-acetyl-D-glucosamine (NAG). The terahertz spectrum in the spectral range from 10 cm^{-1} to 80 cm^{-1} was characterized by a dominant peak at 60 cm^{-1}. On the other hand, the high-resolution ATR-FTIR spectrum from 80 cm^{-1} to 420 cm^{-1} permitted the identification of some additional bands in comparison to those reported in the literature. PM6 Hamiltonian semiempirical calculations, by
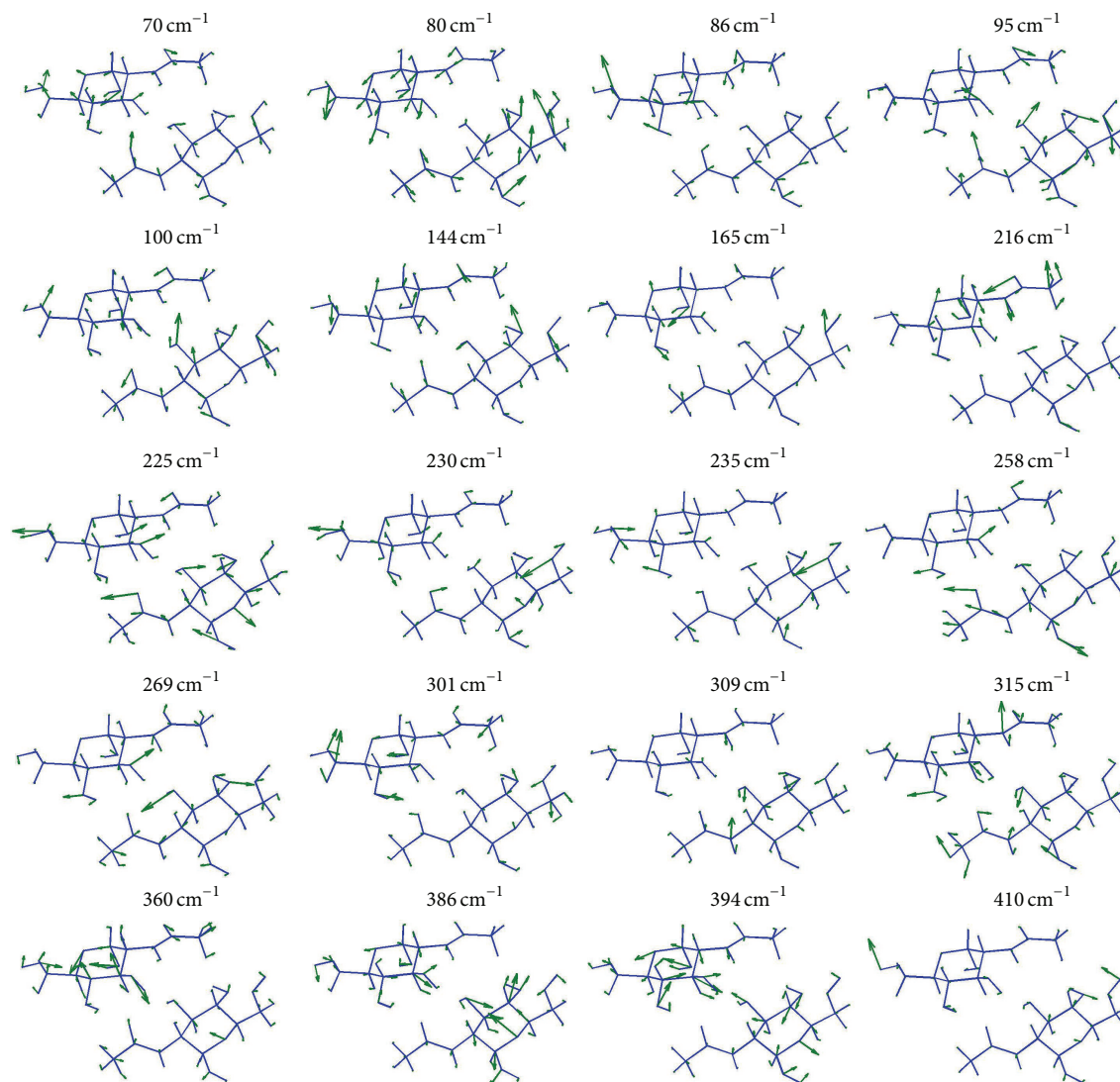
Figure 7: Mass-scaled normal modes of the frequencies in the far infrared spectrum of *N*-acetyl-D-glucosamine.

making use of the recently developed parallel implementations for shared-memory multiprocessor and massively parallel GPU architectures, allowed studying the molecular vibrations at a reduced computation time (*versus* DFT or *ab initio* approaches), obtaining a good qualitative and semiquantitative agreement between the calculated results and the experiments. The largest errors were found for modes with a strong lattice-type vibration contribution, while very good agreement was found when the strongest contributions are due to localized intramolecular vibrations.

Competing Interests

The authors declare that they have no competing interests.

Acknowledgments

References

[1] M. N. V. Ravi Kumar, "A review of chitin and chitosan applications," *Reactive and Functional Polymers*, vol. 46, no. 1, pp. 1–27, 2000.

[2] V. Zargar, M. Asghari, and A. Dashti, "A review on chitin and chitosan polymers: structure, chemistry, solubility, derivatives, and applications," *ChemBioEng Reviews*, vol. 2, no. 3, pp. 204–226, 2015.

[3] V. K. Thakur and M. K. Thakur, "Recent advances in graft copolymerization and applications of chitosan: a review," *ACS*

Sustainable Chemistry and Engineering, vol. 2, no. 12, pp. 2637–2652, 2014.

[4] L. N. Johnson, "The crystal structure of N-acetyl-α-D-glycosamine," *Acta Crystallographica*, vol. 21, no. 6, pp. 885–891, 1966.

[5] C. F. Macrae, P. R. Edgington, P. McCabe et al., "Mercury: visualization and analysis of crystal structures," *Journal of Applied Crystallography*, vol. 39, no. 3, pp. 453–457, 2006.

[6] S. K. Husan, J. B. Hasted, D. Rosen, E. Nicol, and J. R. Birch, "FIR spectra of saccharides and polysaccharides," *Infrared Physics*, vol. 24, no. 2-3, pp. 209–213, 1984.

[7] M. Walther, B. M. Fischer, and P. U. Jepsen, "Noncovalent intermolecular forces in polycrystalline and amorphous saccharides in the far infrared," *Chemical Physics*, vol. 288, no. 2-3, pp. 261–268, 2003.

[8] P. C. Upadhya, Y. C. Shen, A. G. Davies, and E. H. Linfield, "Far-infrared vibrational modes of polycrystalline saccharides," *Vibrational Spectroscopy*, vol. 35, no. 1-2, pp. 139–143, 2004.

[9] A. P. Scott and L. Radom, "Harmonic vibrational frequencies: an evaluation of Hartree-Fock, Møller-Plesset, quadratic configuration interaction, density functional theory, and semiempirical scale factors," *Journal of Physical Chemistry*, vol. 100, no. 41, pp. 16502–16513, 1996.

[10] M. B. Coolidge, J. E. Marlin, and J. J. P. Stewart, "Calculations of molecular vibrational frequencies using semiempirical methods," *Journal of Computational Chemistry*, vol. 12, no. 8, pp. 948–952, 1991.

[11] Z. A. Fekete, E. A. Hoffmann, T. Körtvélyesi, and B. Penke, "Harmonic vibrational frequency scaling factors for the new NDDO Hamiltonians: RM1 and PM6," *Molecular Physics*, vol. 105, no. 19–22, pp. 2597–2605, 2007.

[12] J. D. C. Maia, G. A. Urquiza Carvalho, C. P. Mangueira Jr., S. R. Santana, L. A. F. Cabral, and G. B. Rocha, "GPU linear algebra libraries and GPGPU programming for accelerating MOPAC semiempirical quantum chemistry calculations," *Journal of Chemical Theory and Computation*, vol. 8, no. 9, pp. 3072–3081, 2012.

[13] P. Chamorro-Posada, J. Vázquez-Cabo, F. M. Sánchez-Arévalo et al., "2D to 3D transition of polymeric carbon nitride nanosheets," *Journal of Solid State Chemistry*, vol. 219, pp. 232–241, 2014.

[14] P. Chamorro-Posada, J. Vázquez-Cabo, Ó. Rubiños-López et al., "THz TDS study of several sp2 carbon materials: graphite, needle coke and graphene oxides," *Carbon*, vol. 98, pp. 484–490, 2016.

[15] A. Kovács, B. Nyerges, and V. Izvekov, "Vibrational analysis of *N*-acetyl-α-D-glucosamine and β-D-glucuronic acid," *The Journal of Physical Chemistry B*, vol. 112, no. 18, pp. 5728–5735, 2008.

[16] L. Duvillaret, F. Garet, and J.-L. Coutaz, "A reliable method for extraction of material parameters in terahertz time-domain spectroscopy," *IEEE Journal on Selected Topics in Quantum Electronics*, vol. 2, no. 3, pp. 739–745, 1996.

[17] J. Vázquez-Cabo, P. Chamorro-Posada, F. J. Fraile-Peláez, Ó. Rubiños-López, J. M. López-Santos, and P. Martín-Ramos, "Windowing of THz time-domain spectroscopy signals: a study based on lactose," *Optics Communications*, vol. 366, pp. 386–396, 2016.

[18] J. J. P. Stewart, "Optimization of parameters for semiempirical methods V: modification of NDDO approximations and application to 70 elements," *Journal of Molecular Modeling*, vol. 13, no. 12, pp. 1173–1213, 2007.

[19] J. J. P. Stewart, *MOPAC2012*, Stewart Computational Chemistry, Colorado Springs, Colo, USA, 2012.

[20] G. D. Dean and D. H. Martin, "Inter-molecular vibrations of crystalline polyethylene and long-chain paraffins," *Chemical Physics Letters*, vol. 1, no. 9, pp. 415–416, 1967.

[21] M. Franz, B. M. Fischer, and M. Walther, "The Christiansen effect in terahertz time-domain spectra of coarse-grained powders," *Applied Physics Letters*, vol. 92, no. 2, Article ID 021107, 2008.

[22] J. J. P. Stewart, "Optimization of parameters for semiempirical methods VI: more modifications to the NDDO approximations and re-optimization of parameters," *Journal of Molecular Modeling*, vol. 19, no. 1, pp. 1–32, 2013.

[23] W. Humphrey, A. Dalke, and K. Schulten, "VMD: visual molecular dynamics," *Journal of Molecular Graphics*, vol. 14, no. 1, pp. 33–38, 1996.

[24] P. Chamorro-Posada, "Study of the terahertz spectra of crystalline materials using NDDO semi-empirical methods: polyethylene, poly(vinylidene fluoride) form II and α-D-glucose," https://arxiv.org/abs/1604.03919.